APP Template V1.57 Article id: nano509438 Typesetter: MPS Date received by MPS: 04/02/2015 PE: MAC003313 CE: LE:

IOP Publishing Nanotechnology

Nanotechnology **00** (2015) 000000 (10pp)

Nanoscale conductive pattern of the homoepitaxial AlGaN/GaN transistor

A Pérez-Tomás[1], G Catalàn[1,7], A Fontserè[2], V Iglesias[3], H Chen[4], P M Gammon[4], M R Jennings[4], M Thomas[4], C A Fisher[4], Y K Sharma[4], M Placidi[5], M Chmielowska[6], S Chenot[6], M Porti[3], M Nafría[3] and Y Cordier[6]

[1] The Catalan Institute of Nanoscience and Nanotechnology (ICN2), E-08193 Barcelona, CAT, Spain
[2] ALBA Synchrotron, BP 1413, E-08290 Cerdanyola del Vallès, Barcelona, CAT, Spain
[3] ETSE, Campus UAB, E-08193 Bellaterra, Barcelona, CAT, Spain
[4] School of Engineering, University of Warwick, Coventry CV4 7AL, England, UK
[5] L'Institut de Recerca en Energia de Catalunya (IREC), E-08930, Barcelona, CAT, Spain
[6] CRHEA-CNRS, Rue Bernard Grégory, Sophia Antipolis, F-06560 Valbonne, France
[7] Institut Català de Recerca i Estudis Avançats (ICREA), Barcelona E-08010, CAT, Spain

E-mail: amador.perez@icn.cat

Received 23 December 2014, revised 29 January 2015
Accepted for publication 2 February 2015
Published DD MM 2014

Abstract

The gallium nitride (GaN)-based buffer/barrier mode of growth and morphology, the transistor electrical response (25–310 °C) and the nanoscale pattern of a homoepitaxial AlGaN/GaN high electron mobility transistor (HEMT) have been investigated at the micro and nanoscale. The low channel sheet resistance and the enhanced heat dissipation allow a highly conductive HEMT transistor ($I_{ds} > 1$ A mm^{-1}) to be defined (0.5 A mm^{-1} at 300 °C). The vertical breakdown voltage has been determined to be ~850 V with the vertical drain-bulk (or gate-bulk) current following the hopping mechanism, with an activation energy of 350 meV. The conductive atomic force microscopy nanoscale current pattern does not unequivocally follow the molecular beam epitaxy AlGaN/GaN morphology but it suggests that the FS-GaN substrate presents a series of preferential conductive spots (conductive patches). Both the estimated patches density and the apparent random distribution appear to correlate with the edge-pit dislocations observed via cathodoluminescence. The sub-surface edge-pit dislocations originating in the FS-GaN substrate result in barrier height inhomogeneity within the HEMT Schottky gate producing a subthreshold current.

S Online supplementary data available from stacks.iop.org/NANO/0/000000/mmedia

Keywords: homoepitaxial GaN, high mobility transistor, nanoscale, HEMT, MBE

SQ1 (Some figures may appear in colour only in the online journal)

Q2 ## 1. Introduction

Non-centrosymmetric wurzite (i.e. piezoelectric and pyroelectric) wide direct band-gap (3.4 eV) gallium nitride (GaN) is widely recognized as an outstanding material for solid-state electronic devices, particularly, in the form of the high electron mobility transistor (HEMT) [1]. Blue, white, and blue-violet light-emitting diodes are all based upon GaN semiconductors, providing a wide range of color reproduction in liquid crystal display panels of mobile phones and in a myriad of other smart lighting applications [2]. Furthermore, with naturally enhanced light extraction geometry engineered at the nanoscale, GaN based nano-structures are ideally suited for nanophotonics and optoelectronics [3–5]. Within one-dimensional heterostructures, one may also expect an electron gas at the core/shell interface in a similar fashion to what happens in planar AlGaN/GaN heterojunctions [6]. Most of the applications based on planar structures ultimately require, or will work better, on a homoepitaxial GaN stack. Besides, non-defective homoepitaxial GaN will allow the formation of

vertical devices with theoretical voltage capability over 20 kV that will be a real breakthrough in low emission electrical energy generation, conversion and transportation [7].

The lattice mismatch between non-native substrates (typically silicon, sapphire or silicon carbide) and GaN is particularly problematic for molecular beam epitaxy (MBE) growth, resulting in typical threading dislocation densities between 10^9 and $10^{10}\,cm^{-2}$ [8, 9]. The highest quality GaN epitaxial layers would ideally be achieved by homoepitaxy using a GaN substrate which is identical in crystal structure, lattice constant and thermal expansion coefficient. This homoepitaxy template can be achieved by means of a free-standing (FS-GaN) crystal, (obtained after the growth and separation of several hundred micrometers of GaN on a foreign substrate), but such FS-GaN layers still contains several types of imperfections such as scratches and/or edge pits [10–17]. The inherent FS-GaN defects extend into the HEMT active layers and may degrade the charge transport mechanisms, particularly increasing the HEMT off-state leakage currents which, in turn, reduces the breakdown voltage. The whole fabrication/nano-characterization process is fully detailed; the optimized GaN buffer definition, the HEMT design and fabrication, the extensive electrical and physical homoepitaxial state-of-the-art HEMT characterization and the novel *nanoscale* analysis. Here the homoepitaxial AlGaN/GaN HEMT *nanoscale* morphological features and *nanoscale* conductive pattern will be investigated and correlated with the electronic HEMT electrical performances.

2. Nanoscale homoepitaxial mode of growth and morphology

AlGaN/GaN HEMT layers were grown on thick hydride vapor phase epitaxy FS-GaN (0001) substrates from supplier Lumilog-Saint Gobain where the FS-GaN separation from the foreign substrate (sapphire) results in difficulties such as cracks and other defects [18–28]. The surface of the as-grown FS-GaN substrate cannot be directly used for further epitaxial growth unless a smoothing treatment (mechano-chemical polishing in our case) is performed, which, in turn, can cause further surface and subsurface damage [24]. For subsequent GaN homoeptiaxy it is necessary to compensate the unintentional *n*-type conductivity in the FS-GaN substrate/GaN buffer interface region due to the high incorporation rate of gas phase impurities, primarily oxygen [29] and silicon [30]. For this reason, the AlGaN/GaN HEMT active layers were regrown on an iron-doped (deep acceptors) GaN template. The GaN template consists of 10 μm-thick GaN epilayers grown by low pressure metal organic chemical vapor deposition (MOCVD). These layers were doped with Fe using a Cp_2Fe precursor (ferrocene), resulting in a low dislocation density (DD) ($\sim 10^7\,cm^{-2}$) and highly resistive ($10^{10}\,\Omega\,sq^{-1}$) GaN template. Secondary ions mass spectroscopy revealed a Fe doping level of $1\times10^{19}\,cm^{-3}$. Then, a 1 μm thick undoped GaN buffer was MBE regrown at 780–800 °C using ammonia as the nitrogen precursor in a Riber Compact 21 MBE system. The growth rate for the GaN buffer was $0.6\,\mu m\,h^{-1}$. The

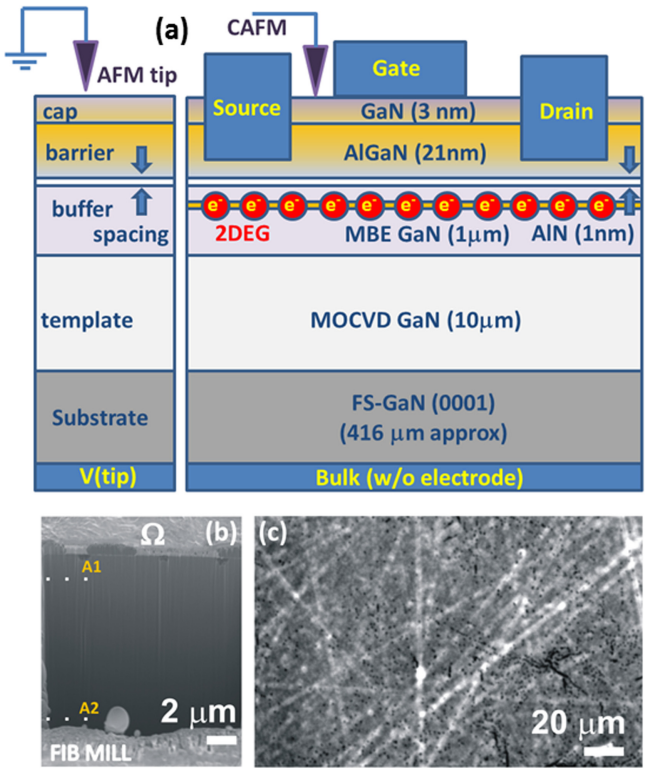

Figure 1. (a) Schematic cross-sectional view of the homoepitaxial HEMT. *A*1 and *A*2 mark the non-visible MBE/MOCVD GaN and MOCVD/FS-GaN interfaces, respectively, which is a signal of good homoepitaxial growth. The Ohmic contact (HEMT drain or source) is referred as Ω. (b) SEM cross-sectional image (54° tilt) formed by FIB milling. The irregular bottom region of the SEM images is due to the ends of the FIB etch (~12 μm milling depth). (c) FS-GaN edge pits and dislocations are revealed with a CL map. The black spots in the CL map arise from the strong nonradiative recombination rate around those edge pits with an estimated density of (CL dark spot count) $1\pm0.3\times10^7\,cm^{-2}$.

HEMT active layer consists in a 1 nm AlN spacer to reduce alloy scattering and to enhance the electron mobility, and a 21 nm undoped $Al_xGa_{1-x}N$ barrier with $x=0.29$ Al mole fraction. Finally, the structure was covered with an additional 3 nm GaN cap layer. The device isolation was achieved by means of a 150 nm deep mesa etch realized by Cl_2/Ar reactive ion etching. Ti/Al/Ni/Au source/drain Ohmic contacts were deposited and annealed for 30 s at 750 °C by rapid thermal annealing. The HEMT gate contact was made with a Ni/Au bi-layer. Source–drain contacts thicknesses are Ti/Al/Ni/Au (15/220/40/50 nm) and gate contact thicknesses are Ni/Au (25/150 nm).

Figure 1(a) depicts a cross-sectional schematic (not to scale) view of the HEMT under investigation. Figure 1(b) shows a cross-sectional (milling by focused ion beam) scanning electron microscopy (SEM) image of the GaN buffer and GaN template. This image shows a cross-sectional view of the homoepitaxial GaN layers on the very top surface (~12 μm) of the structure representing the Ohmic contact, the top MBE AlGaN/GaN HEMT active layers, the 10 μm MOCVD template and the top FS-GaN substrate layers at the bottom. The SEM images show that the interface between the MOVPE

Q3 **Table 1.** Summary of reported dislocation densities for different FS-GaN substrates using several methods such as TEM (transmission electron microscopy) and AFM (atomic force microscopy).

Author	Dislocation density (DD)	Comments	Ref.
Jasinski *et al*	$3 \pm 1 \times 10^7$ cm^{-2} [a]	[a]TEM	[23]
	$4 \pm 2 \times 10^7$ cm^{-2} [b]	[b]plane-view TEM	
	1×10^7 cm^{-2} [c]	[c]EPD	
Grandusky *et al*	8×10^7 cm^{-2}		[24]
Motoki *et al*	1×10^9–1×10^5 cm^{-2}	TEM, CL and EPD (depending on the area)	[25]
Strom *et al*		AFM count	[10]
	8–20×10^7 cm^{-2} [d]	[d]CREE Inc. FS-GaN	
	1×10^7 cm^{-2} [e]	[e]Kyma Inc. FS-GaN	
Lu *et al*	6×10^6 cm^{-2}		[15]
Saitoh *et al*	1×10^6 cm^{-2}	MOCVD GaN	[12]
This work	$1 \pm 0.3 \times 10^7$ cm^{-2} [f]	[f]CL	

[a] TEM.
[b] plane-view TEM.
[c] EPD stands for etch pit density.
[d] CREE Inc. FS-GaN.
[e] Kyma Inc. FS-GaN.
[f] CL stands for cathodoluminescence mapping technique.

overgrown epilayers and the FS-GaN substrate was not visible, indicating the continuous growth of GaN and, correspondingly, a high degree of homoepitaxy.

The DD of the homoepitaxial GaN layers on the FS-GaN substrate was further evaluated by the cathodoluminescence (CL) mapping technique (figure 1(c)), from which a network of scratches in the as-grown sample are evident. This defective region consists of buried defects (scratches and pits), not visible via surface morphology measurement. However, they are certainly visible in optical spectroscopy, which is very sensitive to the recombination occurring at defect sites. Individual dislocations (edge pits) represented by dark spots can be identified in the CL map [31, 32]. The distribution of the edge pits is not uniform thorough the area under investigation. Dwilinski *et al* [33] reported that pits agglomerated mainly along the traces of scratches but we have not observed such a correlation. The DD in the MBE regrown structures was estimated (CL dark spot count) to be $1 \pm 0.3 \times 10^7$ cm^{-2}. The full width at half maximum of GaN x-ray diffraction peaks were 0.032° and 0.087° for (002) and (302) planes which further attests the quality of the layers. This DD value from the CL is in agreement with previous works on GaN MBE/MOCVD epitaxy on FS-GaN substrates (see table 1). Among the lowest reported DD there is no device oriented MBE grown layers. Lu *et al* reported a DD of 6×10^6 cm^{-2} [15] and Saitoh *et al* [12] reported a DD of 1×10^6 cm^{-2} for MOCVD GaN Schottky diodes with a record power figure of merit of 1.7 GW cm^{-2}.

When the HEMT surface is analyzed with SEM and atomic force microscopy (AFM), it is noticeable that the surface was composed of mounds, in the form of a truncated elliptical parabola (figure 2). The mound size distribution is rather uniform with, on average, a base of 1 μm and a height of 5–20 nm (peak to valley distance), typically ~10 nm. Such morphology results from a mixed step flow—2D nucleation growth mode giving rise to kinetic roughening [35]. We believe that the MBE growth temperature is sufficiently low to avoid thickness and composition modulation in the cap and barrier films. The subsurface damage influenced the MOCVD and MBE nucleation and growth, as seen in figure 2. It is believed that the growth was hindered in the areas of subsurface damage. These areas (in the form of scratches) were unable to be completely recovered after the 10 μm of GaN growth. The scratches extend across the entire surface, ranging from 10 to 40 nm deep, as measured by AFM. The introduction of defects in the FS-GaN surface area during the growth and sapphire substrate lift-off can lead to local strain, which effects the epitaxy in these areas. It has been shown that the strain field around dislocations in the SiGe material system can lead to changes in the surface. During epitaxy, this will result in a crosshatch surface morphology representative of the dislocation network [24]. Apart from the mounds and the scratches, another feature is clearly visible on the AlGaN/GaN HEMT surface. As shown in figure 2, nanopipes are clearly a visible morphology feature on the HEMT surface. The presence of nanopipes is commonly reported in the initial stages of the heteroepitaxial growth of GaN (with a density of ~10^8 cm^{-2} and a diameter of 100–200 nm) regardless of the growth method and the substrate used [35, 36]. However, it appears that the reduced lattice mismatch of the homoepitaxial growth mitigates the kinetic roughening process and, therefore, the nanopipes are visible even after 1 μm thick of MBE growth.

3. Homoepitaxial AlGaN/GaN HEMT transistor performances

Despite the complex surface morphology, a very low resistance 2DEG was formed at the GaN buffer/AlGaN barrier heterojunction. The sheet resistance (R_{sh}), the 2DEG concentration (n_s) and the mobility (μ_n) were obtained via Hall measurements, yielding the remarkably low value of $R_{sh} = 270\,\Omega$ sq^{-1} with $n_s = 1.1 \times 10^{13}$ cm^{-2} and

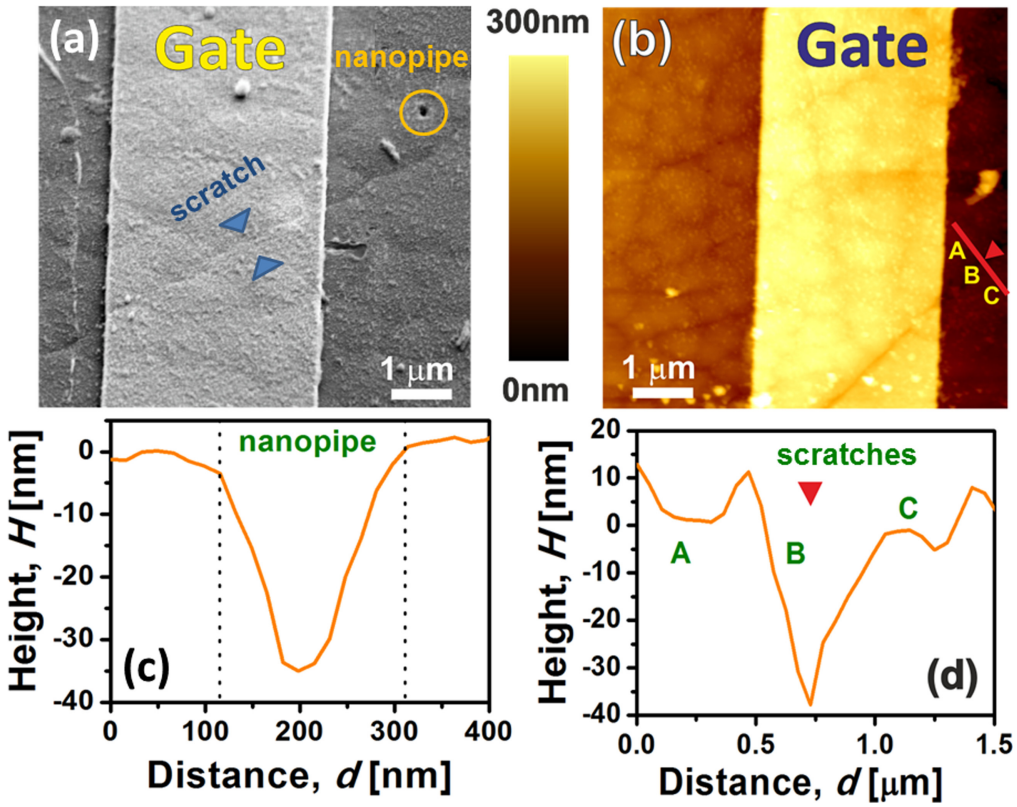

Figure 2. SEM (a) and AFM (b) view of the HEMT gate region. Some surface scratches and nanopipes are visible. (c) Typical nanopipe AFM depth-profile. (d) The scratch valley may reach 40 nm of depth although the device still works.

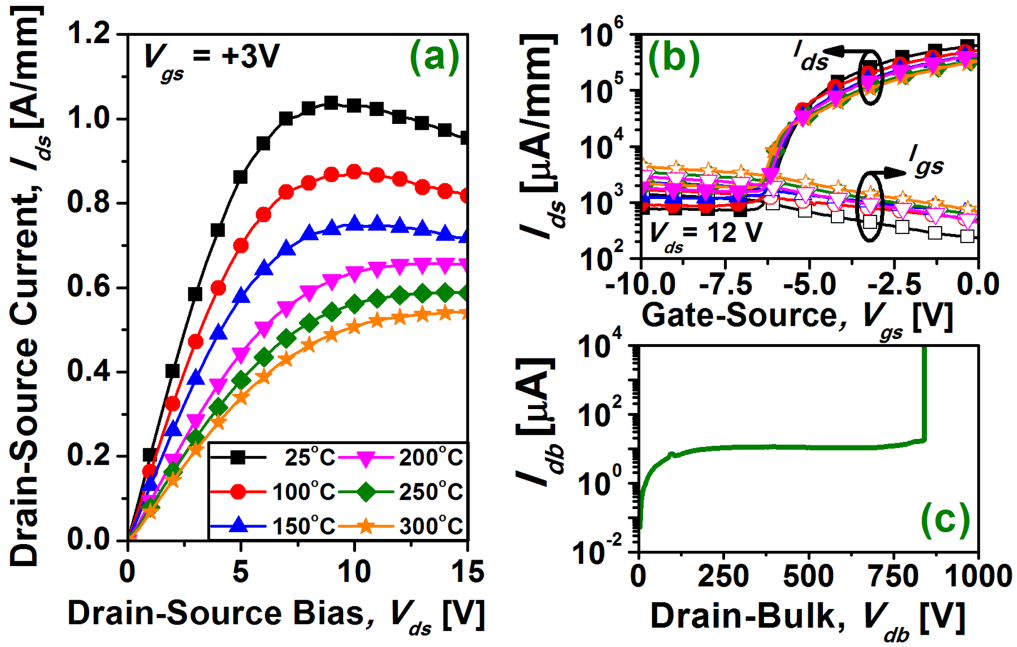

Figure 3. (a) AlGaN/GaN HEMT forward current and (b) transfer curve at varying temperatures (25–300 °C). Drain current exceeding 1 A mm^{-1} was obtained at 25 °C, while this figure drops to 0.5 A mm^{-1} at 300 °C. (c) Vertical bulk current (drain-bulk) showing breakdown phenomena at ~850 V.

$\mu_n = 2110\ \mathrm{cm^2\ V^{-1}\ s^{-1}}$. The particularly low sheet resistance is linked with a reduction of the threading DD during the homoepitiaxial growth [37–40]. The transistor layout was 1.5/2.5/3 μm (source–gate/gate/gate–drain). The device width was 150 μm. The low 2DEG resistivity is the reason for the high level of forward drain–source current given by the HEMT transistor ($I_{ds} > 1$ A mm^{-1}), as shown in figure 3. This value drops by a factor of two to 0.5 A mm^{-1} at 300 °C,

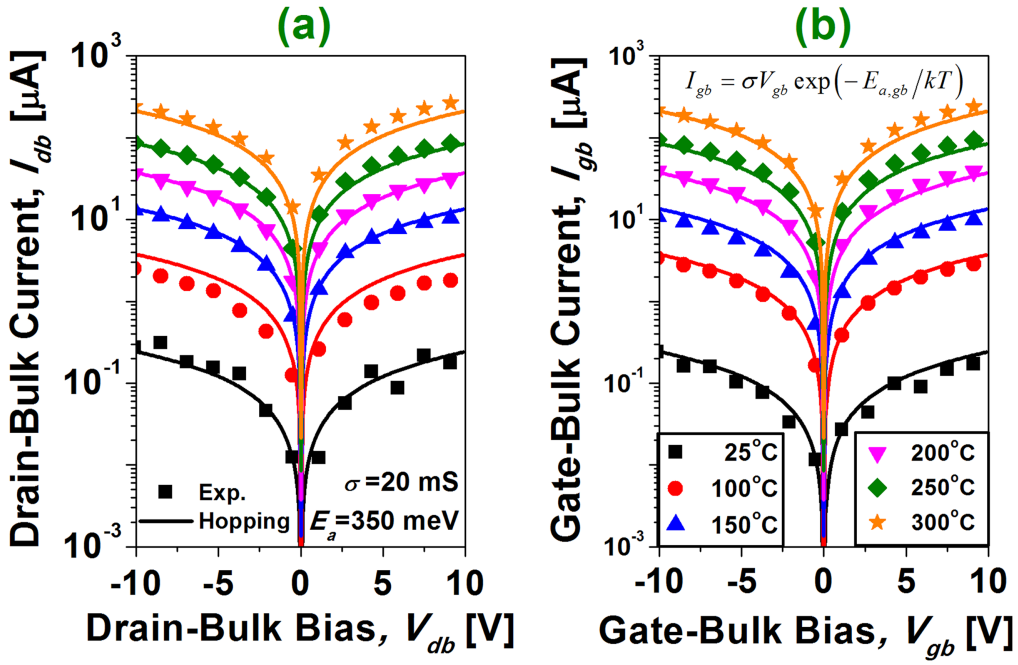

Figure 4. Vertical (a) drain-bulk current (I_{db}) versus V_{db} and (b) gate–drain current (I_{gb}) versus V_{gb}, at varying temperatures (25–300 °C). The bulk-drain/gate are very similar and can be fitted with a hopping mechanism with an activation energy of 350 meV.

though this is still very high. The reduction of I_{ds} with T ($I_{ds} \sim q\mu_n n_s V_{ds}$) is due to the degradation of the electron mobility with T (phonon-scattering increase), although the 2DEG sheet concentration is generally considered as virtually temperature independent [41].

Another relevant characteristic of the AlGaN/GaN FS-GaN HEMT is the reduced thermal effects of the saturation current (figure 3(a)). Self-heating effects may become very relevant on 2DEG sheets because of the large amount of power driven by the channel, (particularly for GaN-on-sapphire). Basically, the self-heating increases the channel temperature to an effective temperature T_{eff}. This effective temperature depends on the dissipated power, the thermal resistance R_{th} and the substrate temperature T_{sub} as $T_{eff} = R_{th} i_{ds} V_{ds} + T_{sub}$. Bulk GaN thermal conductivities larger than 260 W mK^{-1} have recently been reported [40], (the theoretical value for FS-GaN k is as high as 410 W mK^{-1} [42]). In addition, the thermal boundary additional resistance may be naturally mitigated because the homoepitaxy has no heterojunction thermal boundaries [43]. From the negative differential resistance versus T (observed in the saturation drain-forward characteristics of figure 3(a)), the 2DEG effective channel temperature can be estimated to be $T_{eff} = 21.1 + 0.98\,T$ for a dissipated power of 4.7 W mm^{-1} [39]. This means that, due to the improved heat spreading of the FS-GaN substrate at 300 °C, the effective channel temperature was just 5–10% higher than the bulk temperature (for the given dissipated power). To further analyze the effect of the FS-GaN substrate on the HEMT on-state/off-state characteristics, the HEMT drain-bulk current (I_{db}) has also been determined. During the I_{db} versus T tests the HEMT drain was positively biased while the bulk contact was grounded. We have observed that I_{db} basically follows the resistive (hopping) mechanism as, $I_{db} = \sigma_1 V_{db} \exp(-E_{a,db}/kT)$, where σ_1 is the prefactor of the resistive components and $E_{a,db}$ is the activation energy for the resistive component [44] (which can be determined from an Arrhenius plot). The parameters used in the fit were $\sigma_1 = 0.02$ S and $E_{a,db} = 350$ meV. At 25 °C, the drain-bulk current linearly increases with the drain-bulk bias with a typical Ohmic resistance of ~7 MΩ. The destructive breakdown takes place at ~850 V and the I_{db} current was, at the bias before avalanche breakdown, just 9.4×10^{-2} A cm^{-2}.

Therefore, the AlGaN/GaN FS-GaN transistor exhibits outstanding on-state current, high temperature and thermal spreading characteristics and even reasonably vertical high-voltage properties. However, the device also suffers from relatively large drain subthreshold and gate currents, as shown in figure 3(b). The average subthreshold gate–source current (I_{gs}) was typically ~1 mA mm^{-1} at $V_{gs} = -10$ V, the on/off ratio being barely 10^3. This is an indication that the main weakness of the FS-GaN HEMT is the defective nature of the gate Schottky contact. It must be mentioned that although the high quality GaN homoepitaxial growth is a hot topic, (which is succinctly summarized in table 1), only a very small minority of these papers actually reports on a final device (HEMT) on these homoepitaxial structures, and virtually no-one of them is reporting any power management features such as the vertical breakdown voltage or the high temperature behavior (25–300 °C). To further investigate this we have comparatively performed drain-bulk and gate-bulk (I_{gb}) versus T measurements as shown in figure 4. The FS-GaN substrate was grounded during the test. For the drain–gate configuration, one should expect a forward current ($+V_{gb}$) increase following the thermionic flow of electrons over the metal-semiconductor barrier, but this was mitigated by the FS-GaN and GaN buffer resistive templates. Applying reverse

bias ($-V_{gb}$) to the gate, one should expect that the thermionic emission over the Schottky barrier makes only a negligible contribution to reverse-bias current flow due to the large barrier heights typical for Schottky contacts to GaN and, hence, the I_{gb} should present a typical rectifying characteristic. Therefore, the Ohmic-like I_{gd} behavior is again an indication of AlGaN defective paths presenting reduced Schottky barrier height. The gate-bulk current was again fitted with the hopping expression as $I_{gb} = \sigma_2 V_{gb} \exp\left(-E_{a,gb}/kT\right)$, with $\sigma_2 = 0.02$ S and $E_{a,gb} = 350$ meV. These results suggest that there is a common mechanism that is responsible for the I_{gb} and I_{db} leakage paths in the AlGaN/GaN/FS-GaN heterostructure and thus, (as the I_{db} take into account the leakage current between the 2DEG and the back contact), it should be related to some of the extending defects from the GaN buffer into the AlGaN barrier. This is further investigated in the next section by means of the conductive AFM (CAFM) technique.

4. Homoepitaxial HEMT conductive scanning probing at the nanoscale

FS-GaN presents a natural vertical architecture for CAFM to be carried out when compared with a typical heteroepitaxial GaN wafer. It is well know that there are many threading dislocations in the MBE AlGaN/GaN HEMT epitaxial layers (typically 10^8–10^9 cm^{-2}). Most of them are normal to the HEMT active area forming the boundaries of the network of the sub-grains which enable the conductive vertical path. It has been widely suggested in the literature [45–53] that a link exists between leakage current and threading dislocations but only very few works investigate this at the nanoscale [51–53].

To determine the nanoscale conductive pattern of the homoepitaxial MBE HEMT, we have performed an extensive CAFM analysis on 20–25 different locations (with different scanning areas ranging from 1×1 to $10 \times 10\ \mu$m^2) carried out in four different experiments (different days and new AFM tip each time). The CAFM measurements were carried out with an AFM Agilent 5100 (from Scientec), equipped with a conductive tip and a picoamplifier with an overall amplification of 10^{12} V A^{-1}. An additional pA booster provided low pass filtering with a bandwidth of 400 Hz. The voltage output of the pA booster is sampled by the analog–digital converter of the AFM controller with a sampling rate of 65 kHz, yielding a rms noise level <30 fA. In this work, we have used silicon tips coated by a metallic layer of Co/Cr and bulk diamond tips doped with boron. The scan was performed in contact mode at a frequency of 0.5 Hz. In these experiments, the surface was scanned with the tip grounded, applying a negative bias between to the back contact. The regions under study were the gate–drain spacing (L_{gd}) of large HEMTs, with varying L_{gd}. There the GaN top cap layer was accessible. Individual *I*–*V* probing with the AFM tip has revealed that no appreciable current was observed for substrate biases smaller than ~7.5 V. The CAFM maps presented in this section are then performed at substrate bias of 10 V (being the maximum bias of our setup). The CAFM maps were analyzed with specialized software [54].

In general, the vertical nanoscale current shows several clear features: (i) it does not follow the MBE GaN cap/AlGaN morphology and (ii) the current pattern is rather composed by a series of randomly distributed conductive spots, the density of which has been determined to be as high as $\sim 9 \times 10^9$ cm^{-2}. The distribution (grain distribution versus equivalent grain radius *r*) of *small* conductive spots (typically $r \sim$5–25 nm) has been determined to be approximated by an exponential distribution function $f(r) = \sigma_r^2 \exp(-r/r_c)$ with $\sigma_r = 17.19$ and a characteristic radius of $r_c = 4.3$ nm ($1 \times 1\ \mu$m^2 sample). A small number of conductive spots present larger sizes being outside of the distribution function on the largest *r* limit (*large* conductive patches). Shown in figure 5 are the CAFM scans of the homoepitaxial HEMT surface and the superimposed current map versus topography for a $10 \times 10\ \mu$m^2 scan biased at −10 V (figure 5(b)). Dark spots represent the highly conductive patches distributed all over the surface. The average diameter of the *large* conductive patches is ~98 nm although peaks with diameters of 100–140 nm also take place, but at lower frequency. The average *small* patches have a diameter of 22–28 nm and they are five times more frequent than the large ones. For the majority of the peaks, the maximum current is not larger than 0.18 nA (which would correspond to the *small* patches). The maximum current peak observed was 3.5 nA, which corresponds to the vertical scale of figure 5(c). In any case, there is no unequivocal correlation between enhanced conductivity spots, and areas of scratches, the top of the mounds and/or inter-mounds [55]. Simpkins *et al* [51] observed (CAFM GaN-on-sapphire) that every leakage path coincided with a growth hillock (but only ~10% of hillocks conducted), which was believed to grow spirally about a screw or mixed dislocation located at the center [55]. As can be clearly observed in figure 6(f), there is no correlation again between the nanoscale CAFM current (*small* or *large* spots) and the spiral hillocks distribution for our samples. Therefore, the nanoscale current pattern would suggest that the FS-GaN substrate presents a series of preferential conductive spots which seems to be transferred across the MOCVD template and the MBE buffer layer, as vertical conductive *large* patches. Both the estimated *large* patches density (10^8–10^7 cm^{-2}) and the apparent random distribution correlates well with the edge pits observed in the cathodeluminescence measurement shown in figure 1(c). It is then possible to suggest that the (hopping) vertical HEMT current (shown in figure 3(c)) is established primarily by these *large* conductive patches. With an estimated (onset of the breakdown) current density of $J_{db} \sim 9.4 \times 10^{-2}$ A cm^{-2} (~840 V) only a small portion (~0.01%) of the device area (1.8×10^{-4} cm^2) would actually contributing to the current flow through the different large patches. It was observed that the MBE nanopipes (with a diameter typically ~400 nm) have generally a hexagonal geometry as shown in figure 6(a). Hexagonal pits have been already reported in particular after hot acid exposure caused by the different etching rates of different facets [57]. GaN hexagonal pits have also been described previously as open core screw dislocations [58]. A detailed scan of any nanopipe

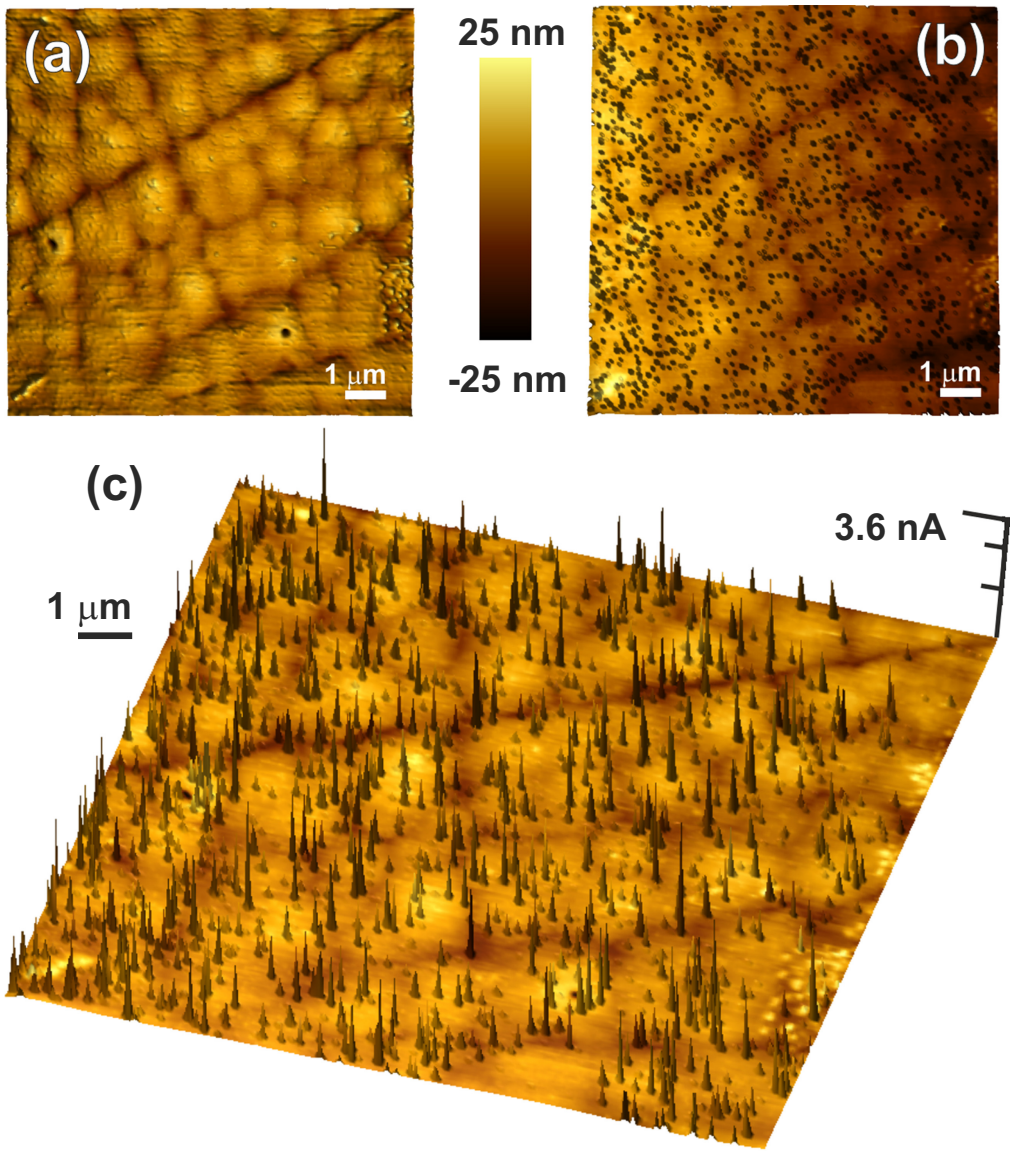

Figure 5. Conductive AFM scans of the homoepitaxial HEMT surface in the drain–gate spacing with (a) topography and (b) current map versus topography of surface taken with the CAFM for a $10 \times 10\ \mu m^2$ scan biased at −10 V. Dark regions represent the high conductive spots distributed all over the surface. (c) 3D view of (b). The vertical current scale is 0–3.6 nA.

vicinity clearly shows that they are not particularly conductive (figure 6(b)). Indeed an increase of the current was observed at the edges of a hexagonal nanopipe, as shown in figure 6(d), but the current spike is by far lower than those that can be observed on the regular surface. Therefore, nanopipes are not the HEMT gate current killing defect as one could presume just looking at the surface. Regarding the vertical breakdown voltage, the most critical defect appears to be the edge-pits dislocations extending from the FS-GaN substrate. Besides, the associated small nanopillar current paths can contribute to the HEMT subthreshold gate current likely getting electrons from the 2DEG.

The microscale reverse characteristic of the AlGaN barrier is depicted in figure 3(b). If we assume that 2DEG is formed and there is an ohmic contact between the source and the 2DEG acting, in turn, as the back parallel plate of a capacitor, the gate–source current (i_{gs}) is, in fact, the current flowing from the 2DEG into the Ni Schottky gate metal (and viceversa). Remarkably, even displaying much lower DD at the nanoscale, this i_{gs} is several orders of magnitude higher ($\sim 10^3\ \mu A\ mm^{-1}$) than the typical value for a similar AlGaN barrier grown on silicon or sapphire [59]. Another interesting fact is revealed when analyzing the microscale vertical current (shown in figures 4(a) and (b)). Bulk drain and gate currents (i.e. i_{db} and i_{gb}) are both linear (Ohmic) although the conductivity is low. This again is clear indication of poor Schottky rectifying characteristics in the vicinity of the metal electrodes. Analogously, also remarkable is the fact of virtually no difference at the microscale between i_{db} (figure 4(a)) and i_{gb} (figure 4(b)) suggesting a thin or defective Schottky gate depletion region. A network of dislocations can act as line charge towards the bulk semiconductor having small barrier height and/or barrier width on the nanoscale. This sparse (DD is low as $10^7\ cm^2$) but low barrier inhomogeneous

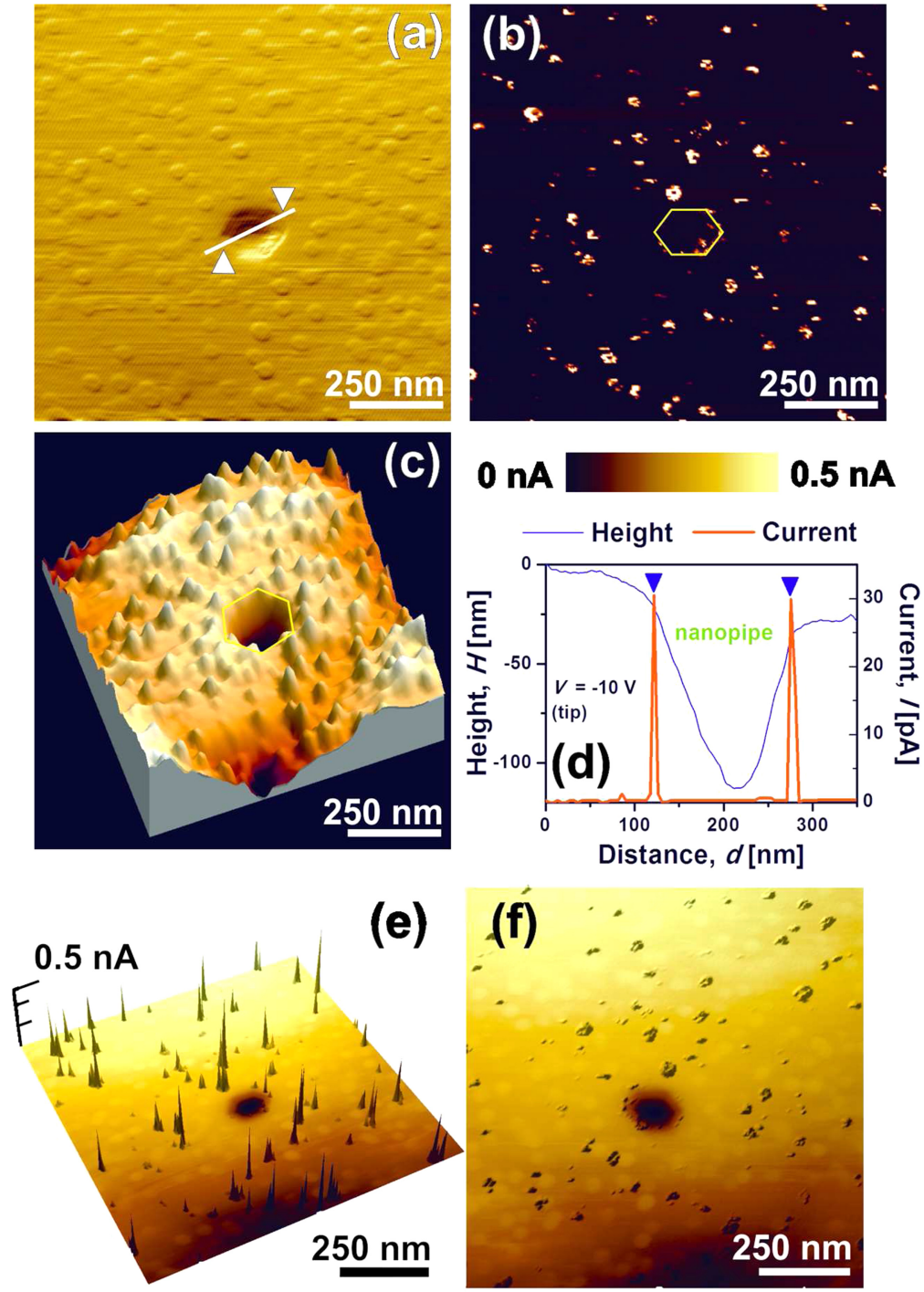

Figure 6. Conductive AFM scans of a detail of the homoepitaxial HEMT surface with (a) topography (3D view in (c)) and (b) current map taken with the CAFM for a $1 \times 1\ \mu m^2$ scan biased at −10 V. (d) Respective cross-sectional profiles along the solid line marked in (a). The nanopipe current is larger in the edge region of the hexagonal pit. However, the hexagonal nanopipe is not particularly conductive as it is shown in the superposed topography/current maps (e) and (f).

patch network of around 10 line charges for every 10 square microns would be in the basis of the vertical leakage current. The nanoscale pattern in the form of a small density of small/large conductive patches correlates well with the anomalously high (when compared with silicon or sapphire) subthreshold gate current. As the Ohmic-like bulk current is low ($\sim 0.1\ \mu A\ mm^{-1}$), it would indicate that the density of conductive dislocations is higher in the vicinity of the electrodes but vanishing towards the template bulk. This would explain why the MOCVD template is efficient in the suppression of the FS-GaN vertical currents (relatively larger breakdown voltages larger than 800 V can be achieved) even in the presence of persistent lateral HEMT sub-threshold currents.

In summary, these results suggest that, effectively, excellent AlGaN/GaN transistors can be defined on homoepitaxial GaN substrates. However, the transistor's Schottky

gate inherits some of sub-surface edge-pit dislocations from the FS-GaN substrate, causing barrier height inhomogeneity.

5. Conclusions

The MOCVD/MBE nanoscale homoepitaxial AlGaN/GaN/FS-GaN HEMT mode of growth was investigated showing mounds, scratches, nanopipes, hillocks and edge pits. Despite the complex surface morphology, a very low resistance 2DEG was formed with $R_{sh} = 270\,\Omega\,sq^{-1}$, $n_s = 1.1 \times 10^{13}\,cm^{-2}$ and $\mu_n = 2110\,cm^2\,V^{-1}\,s^{-1}$. The low 2DEG R_{sh} and the homoepitaxial enhanced heat dissipation allows a highly conductive HEMT transistor ($I_{ds} > 1\,A\,mm^{-1}$) to be defined, which is also able to deliver large currents at very high temperature ($0.5\,A\,mm^{-1}$ at 300 °C). The vertical homoepitaxial HEMT bulk current basically follows the hopping mechanism with activation energy of 350 meV and V_B ~850 V. The *nanoscale* current (CAFM) does not follow the AlGaN/GaN HEMT morphology but is rather composed by a series of randomly distributed conductive spots (*small* and *large* patches depending on their characteristic size). The average diameter of the *large* conductive patches is 85–98 nm. The *small* patches have an average diameter of 22–28 nm and they are (at least) five times more frequent than the *large* patches. For the majority of the *small* conductive spots the maximum current is not larger than 0.18 nA, but the *large* patches may present nanoscale currents in the 1–3 nA range. The estimated *large* patches density (10^8–$10^7\,cm^{-2}$) and the apparent random distribution correlate with the edge pits observed in a CL measurement suggesting that the vertical HEMT current mechanism and breakdown is primarily established by these *large* conductive patches. Besides, the transistor Schottky gate would inherit some of the FS-GaN substrate sub-surface edge-pits dislocations in the form of low barrier height inhomogeneities.

Acknowledgments

ICN2 acknowledges support of the Spanish MINECO through the Severo Ochoa Centers of Excellence Program under Grant SEV-2013-0295.

References

[1] Mishra U K, Shen L, Kazior T E and Wu Y F 2008 *Proc. IEEE* **96** 287
[2] Choi J H *et al* 2011 *Nat. Photonics* **5** 763
[3] Jeon D W, Choi W M, Shin H J, Yoon S M, Choi J Y, Jang L W and Lee I H 2011 *J. Mater. Chem.* **21** 17688
[4] Deb P, Kim H, Qin Y, Lahiji R, Oliver M, Reifenberger R and Sands T 2006 *Nano Lett.* **6** 2893
[5] Schuster F, Furtmayr F, Zamani R, Magén C, Morante J R, Arbiol J, Garrido J A and Stutzmann M 2012 *Nano Lett.* **12** 2199
[6] Wong B M, Léonard F, Li Q and Wang G T 2011 *Nano Lett.* **11** 3074
[7] Uemoto Y *et al* 2007 *IEEE IEDM* p 861
Srivastava P *et al* 2011 *IEEE Electron Device Lett.* **32** 30
[8] Nakamura S 1998 *Science* **281** 956
[9] Pearton S J, Ren F, Zhang A P and Lee K P 2000 *Mater. Sci. Eng.* **R30** 55
Polyakov A Y, Pearton S J, Frenzer P, Ren F, Liuc L and Kim J 2013 *J. Mater. Chem.* C **1** 877
[10] Storm D F, Katzer D S, Mittereder J A, Binari S C, Shanabrook B V, Xu X, McVey D S, Vaudo R P and Brandes G R 2005 *J Cryst. Growth* **281** 32
Storm D F, Katzer D S, Roussos J A, Mittereder J A, Bass R, Binari S C, Hanser D, Preble E A and Evans K R *J. Cryst. Growth* 2007 **301–2** 429
[11] Kanechika M, Sugimoto M, Soejima N, Ueda I, Ishiguro O, Kondama M, Hayashi E, Itoh K, Uesugi T and Kachi T 2007 *Japan. J. Appl. Phys.* **46** L503
[12] Saitoh Y, Sumiyoshi K, Okada M, Horii T, Miyazaki T, Shiomi H, Ueno M, Katayama K, Kiyama M and Nakamura T 2010 *Appl. Phys. Express* **3** 081001
[13] Zhang A P, Johnson J W, Luo B, Ren F, Pearton S J, Park S S, Park Y J and Chyi J I 2001 *Appl. Phys. Lett.* **79** 1555
[14] Irokawa Y *et al* 2003 *Appl. Phys. Lett.* **83** 2271
[15] Lu H, Zhang R, Xiu X, Xie Z, Zheng Y and Li Z 2007 *Appl. Phys. Lett.* **91** 172113
[16] Faraz S M, Ashraf H, Imran Arshad M, Hageman P R, Asghar M and Wahab Q 2010 *Semicond. Sci. Technol.* **25** 095008
[17] Wang Y *et al* 2011 *Semicond. Sci. Technol.* **26** 022002
[18] Kachel K *et al* 2012 *Cryst. Eng. Comm.* **14** 8536
[19] Bejtka K, Martin R W, Watson I M, Ndiaye S and Leroux M 2006 *Appl. Phys. Lett.* **89** 191912
[20] Kim-Chauveau H *et al* 2012 *J. Cryst. Growth* **338** 20
[21] Miskys C R, Kelly M K, Ambacher O and Stutzmann M 2003 *Phys. Status Solidi* c **0** 1627
[22] Martinez-Criado G, Kuball M, Benyoucef M, Sarua A, Frayssinet E, Beaumont B, Gibart P, Miskys C R and Stutzmann M 2003 *J. Cryst. Growth* **255** 277
[23] Jasinski J, Swider W, Liliental-Weber Z, Visconti P, Jones K M, Reshchikov M A, Yun F, Morkoc H, Park S S and Lee K Y 2001 *Appl. Phys. Lett.* **78** 2297
[24] Grandusky J R, Jindal V, Tripathi N, Shahedipour-Sandvik F, Lu H, Kaminsky E B and Melkote R 2007 *J. Cryst. Growth* **307** 309
[25] Motoki K *et al* 2002 *J. Cryst. Growth* **237–9** 912
[26] Wei T B, Duan R F, Wang J X, Li J M, Huo Z Q, Ma P, Liu Zh. and Zeng Y P 2007 *Appl. Surf. Sci.* **253** 7423
[27] Chen K M, Wu Y H, Yeh Y H, Chiang C H, Chen K Y and Lee W I 2011 *J. Cryst. Growth* **318** 454
[28] Cao X A, Lu H, Kaminsky E B, Arthur S D, Grandusky J R and Shahedipour-Sandvik F 2007 *J. Cryst. Growth* **300** 382
[29] Zhu T and Oliver R A 2012 *Phys. Chem. Chem. Phys.* **14** 9558
[30] Cordier Y, Azize M, Baron N, Chenot S, Tottereau O and Massies J 2007 *J. Cryst. Growth* **309** 1
[31] Albrecht M, Weyher J L, Lucznik B, Grzegory I and Porowski S 2008 *Appl. Phys. Lett.* **92** 231909
[32] Lu L *et al* 2008 *J. Appl. Phys.* **104** 123525
[33] Dwilinski R, Doradzinski R, Garczynski J, Sierzputowski L P, Zajac M and Rudzinski M 2009 *J. Cryst. Growth* **311** 3058
[34] Burton W K, Cabrera N and Frank F C 1951 *Phil. Trans. R. Soc.* A **243** 299
[35] Vézian S, Natali F, Semond F and Massies J 2004 *Phys. Rev.* B **69** 125329
[36] Corrion A L, Poblenz C, Wu F and Speck J S 2008 *J. Appl. Phys.* **103** 093529
[37] Chu K K *et al* 2004 *IEEE Electron Device Lett.* **25** 596
[38] Kaun S W, Hoi Wong M, Mishra U K and Speck J S 2012 *Appl. Phys. Lett.* **100** 262102

[39] Fontserè A, Pérez-Tomás A, Placidi M, Baron N, Chenot S, Moreno J C and Cordier Y 2013 *Electrochem. Solid-State Lett.* **2** P4
[40] Killat N *et al* 2012 *IEEE Electron Device Lett.* **33** 366
[41] Pérez-Tomás A, Placidi M, Baron N, Chenot S, Cordier Y, Moreno J C, Constant A, Godignon P and Millán J 2009 *J. Appl. Phys.* **106** 074519
Pérez-Tomás A, Placidi M, Perpiñà X, Constant A, Godignon P, Jordà X, Brosselard P and Millán J 2009 *J. Appl. Phys.* **105** 114510
[42] Witek A 1998 *Diam. Relat. Mater.* **7** 962
[43] Manoi A, Pomeroy J W, Killat N and Kuball M 2010 *IEEE Electron Device Lett.* **31** 1395
[44] Lo C F, Kang T S, Liu L, Chang C Y, Pearton S J, Kravchenko I I, Laboutin O, Johnson J W and Ren F 2010 *Appl. Phys. Lett.* **97** 262116
[45] Roccaforte F, Iucolano F, Alberti A, Giannazzo F, Puglisi V, Bongiorno C, Di Franco S and Raineri V 2006 *Superlattices Microstruct.* **40** 373
[46] Leconte S, Monroy E and Gérard J M 2006 *Superlattices Microstruct.* **40** 507
[47] Fontserè A *et al* 2011 *Appl. Phys. Lett.* **99** 213504
[48] Yu E T, Waltereit P and Speck J 2003 *J. Appl. Phys.* **94** 1448
[49] Weimann N G, Eastman L F, Doppalapudi D, Ng H M and Moustakas T D 2008 *J. Appl. Phys.* **103** 093529
[50] Hsu J W P, Manfra M J, Lang D V, Richter S, Chu S N G, Sergent A M, Kleiman R N, Pfeiffer L N and Molnar R J 2002 *Appl. Phys. Lett.* **81** 79
[51] Simpkins B S, Yu E T, Waltereit P and Speck J 2003 *J. Appl. Phys.* **94** 1448
[52] Fontserè A *et al* 2012 *Appl. Phys. Lett.* **101** 093505
[53] Zhang H, Miller E J and Yu E T 2006 *J. Appl. Phys.* **99** 023703
[54] Horcas I, Fernandez R, Gomez-Rodriguez J M, Colchero J, Gomez-Herrero J and Baro A M 2007 *Rev. Sci. Instrum.* **78** 013705
Nečas D and Klapetek P *Cent. Eur. J. Phys.* 2012 **10** 181
[55] Ho C H, Lien D H, Chang H C, Lin C A, Kang C F, Hsing M K, Lai K Y and He J H 2012 *Nanoscale* **4** 7346
[56] Strunk H P 1996 *J. Cryst. Growth* **160** 184 Q5
[57] Basilio A M *et al* 2010 *J. Mater. Chem.* **20** 8118
[58] Mathis S K, Romanov A E, Chen L F, Beltz G E, Pompe W and Speck J S 2001 *J. Cryst. Growth* **231** 371
[59] Fontserè A, Pérez-Tomás A, Placidi M, Baron N, Chenot S, Moreno J C, Rennesson S and Cordier Y 2013 *Appl. Phys. Lett.* **102** 093503